Physical Layer Security: Detection of Active Eavesdropping Attacks by Support Vector Machines

Tiep M. Hoang, Trung Q. Duong, *Senior Member, IEEE*, Hoang Duong Tuan, Sangarapillai Lambotharan, *Senior Member, IEEE*, Emi Garcia-Palacios, *Member, IEEE*, and Long D. Nguyen

***Abstract*—This paper presents a framework for converting wireless signals into structured datasets, which can be fed into machine learning algorithms for the detection of active eavesdropping attacks at the physical layer. More specifically, a wireless communication system, which consists of K legal users, one access point (AP) and one active eavesdropper, is considered. To cope with the eavesdropper who breaks into the system during the uplink phase, we first build structured datasets based on several different features. We then apply support vector machine (SVM) classifiers and one-class SVM classifiers to those structured datasets for detecting the presence of eavesdropper. Regarding the data, we first process received signals at the AP and then define three different features (i.e., MEAN, RATIO and SUM) based on the post-processing signals. Noticeably, our three defined features are formulated such that they have relevant statistical properties. Enabling the AP to simulate the entire process of transmission, we form the so-called artificial training data (ATD) that is used for training SVM (or one-class SVM) models. While SVM is preferred in the case of having perfect channel state information (CSI) of all channels, one-class SVM is preferred in the case of having only the CSI of legal users. We also evaluate the accuracy of the trained models in relation to the choice of kernel functions, the choice of features, and the change of eavesdropper's power. Numerical results show that the accuracy is relatively sensitive to adjusting parameters. Under some settings, SVM classifiers (or even one-class SVM) can bring about the accuracy of over 90%.**

***Index terms*—**Physical layer security, active eavesdropping, machine learning, support vector machine (SVM), one-class SVM, artificial training data.

I. Introduction

Over the last few years, we have witnessed an increasing interest in the topic of physical layer security (PLS) in wireless communication systems (WCSs). Different from security methods at upper layers, the PLS relies on the random nature of wireless channels in order to deal with eavesdroppers [1]. In the context of PLS, two different types of eavesdroppers are often discussed: i) passive eavesdroppers who only listen and ii) active eavesdroppers who break into WCSs by impersonating legal users. It is shown that an active eavesdropper is more dangerous than a passive one, because the amount of information leaked to the active eavesdropper is larger [2]–[5]. So far, numerous works have been conducted to deal with active eavesdropping. One of the promising solutions is the detection of eavesdroppers' presence.

In fact, if a transmitter is not aware of the eavesdroppers' presence, then it might naively broadcast signals without a doubt. If this transmitter becomes wiser and is aware of security risks, then it can generate artificial noise to interfere with eavesdroppers but this method consumes a portion of power budget [6]. On the contrary, if a transmitter can detect eavesdroppers, then it can design more suitable strategies to deal with eavesdroppers. In short, intrusion detection is a matter of importance that needs to be addressed in all security problems as a whole and in PLS-related problems in particular.

Among the most attractive topics are the methods of wireless network intrusion detection. For example, [7] suggests using carrier frequency offset (CFO) along with Kalman filtering, and [8] suggests channel probing and hypothesis testing. However, machine learning is out of the context of these works. Also in need of detecting network intruders, recent works pay attention to the application of machine learning due to its huge potential in the era of big data and fifth generation (5G) networks. For example, [9] uses Q-learning and Dyna-Q in combination with game theory. Meanwhile, [10] applies Q-learning, which is a reinforcement learning technique, to the PLS in vehicular ad-hoc networks. In [11], extreme learning machine, which is an algorithm for *single hidden layer* feedforward neural networks, has been introduced and contributed to the field recently. The work in [12] considers two types of supervised learning (i.e., support vector machine (SVM) and Fisher's linear discriminant analysis (Fisher's LDA)) to classify channels in order to identify the eavesdropper's channel. SVM is also applied to the PLS in smart grid in [13], while in-situ machine learning is applied in [14]. In short, a range of different machine learning algorithms has been applied to the PLS in WCSs.

Having said that, the investigations are incomplete, and many PLS-related aspects remain lacking. The works in [9]–[14] do not consider wireless propagation models (i.e., the relation between transmitted signals and received signals through wireless channels); thus, there is no understanding of transmitting and receiving signals. In fact, these works fail to show the way signals are processed and the way data

T. M. Hoang was with the School of Electronics, Electrical Engineering and Computer Science, Queen's University Belfast, Belfast BT7 1NN, UK. He is now with the School of Electronics and Computer Science, University of Southampton, Southampton, SO17 1BJ, UK (e-mail: tiep.hoang@soton.ac.uk).

T. Q. Duong, and E. Garcia-Palacios are with the School of Electronics, Electrical Engineering and Computer Science, Queen's University Belfast, Belfast BT7 1NN, UK (e-mail: trung.q.duong@qub.ac.uk, e.garcia@ee.qub.ac.uk).

H. D. Tuan is with the University of Technology Sydney, Ultimo, NSW 2007, Australia (e-mail: tuan.hoang@uts.edu.au).

S. Lambotharan is with the Wolfson School of Mechanical, Manufacturing and Electrical Engineering, Loughborough University, United Kingdom (e-mail: S.Lambotharan@lboro.ac.uk).

L. D. Nguyen is with Duy Tan University, Da Nang 550000, Vietnam (e-mail: nguyendinhlong1@duytan.edu.vn).

is collected from wireless signals. Only [15] relates wireless propagation to data that is fed to machine learning algorithms. Similar to [15], we also consider the transmission process with the relation between transmitted and received signals, and then create data from the received signals. Unlike [15] that uses Gaussian mixture models for classification tasks, we use SVM models and one-class SVM (OC-SVM) models in this paper.

When it comes to creating features for data from wireless signals, the cited works [10]–[14] suggest several approaches to detecting eavesdroppers. For example, [10] suggests using received signal strength (RSS) indicator, MAC address, and arrival time of a packet as three features of a data point. [12] also considers three features including arrival time. The two remaining features defined in [12] are based on RSS and Z-transform. In [11], the feature space is constructed based on formulating the Pearson correlation coefficient and the Euclidean distance between two samples. In [13], each feature has a certain distribution that is fitted to preprocessed data. While [15] considers channel estimation and use the normalized magnitudes of estimated channels as the features of input data. Besides, in-phase and quadrature (I-Q) components along with CFO can also be used to create features [14]. However, so far there have not been any standard frameworks for building the features of a dataset, especially in the joint topic of PLS and machine learning. This leads to a gap between the PLS and machine learning. Accordingly, a question arises: how wireless PLS signals can be processed before being entering into a machine learning algorithm for intrusion detection? Since the data is among the most important pillars of machine learning [16], it is necessary to answer this question.

In this work, we present a framework of creating the data from wireless PLS signals such that all the features of the data have statistical properties. Using the newly-created data, we detect active eavesdropping attacks with the help of SVM and OC-SVM. From a PLS-related point of view, this paper is pioneering in using SVM and OC-SVM models for intrusion detection in WCSs. Specifically, our contributions can be listed as follows.

- We process the received signals by transforming them into a *structured dataset*, which consists of three different features (namely, MEAN, RATIO and SUM). The features are formulated such that they are associated with certain constants. Moreover, data points in a feature column satisfy the requirement that the newer data point, the closer to the corresponding constant it reaches (especially when compared to the oldest data points).
- In relation to training data, we build up the so-called *artificial training data* (ATD). Based on the channel state information (CSI) of channels, we formulate two types of the ATD. If the CSI of eavesdropping channel is known, then the ATD with two classes will be formulated and then be used for training SVM models. If the CSI of eavesdropping channel is unknown, the ATD with only one class will be formulated and then be used for OC-SVM models. Noticeably, the ATD introduced in this paper can also be fed to other types of supervised learning and unsupervised learning models.
- Respectively using SVMs and OC-SVMs, we evaluate the performance of our approach to detecting eavesdropper's attacks. Comparing four different kernel functions, we point out the most stable kernel function that is least affected by the change of SVM (and/or OC-SVM) coefficients , and the worst kernel function that changes fast with SVM (and/or OC-SVM) coefficients.
- We show that the probability of successful detection increases with the eavesdropper's power. In parallel, we present the relation between the eavesdropper's power and the selection of SVM (and/or OC-SVM) parameters.

TABLE I
NOTATION

Symbols	Meanings
$\mathcal{R}$, $\mathcal{H}$	Input space and feature space, respectively.
$\phi(\mathbf{x}_s)$	The image of a training sample $\mathbf{x}_s$ in $\mathcal{H}$.
$\mathcal{K}(\mathbf{x}_s, \mathbf{x})$	The kernel function that computes the inner products between $\phi(\mathbf{x}_s)$ and $\phi(\mathbf{x})$ in $\mathcal{H}$.
C	The regularization parameter in SVM.
γ	The parameter that appears in kernel functions, e.g., radius basis function (RBF), polynomial, and sigmoid kernels.
$\left\{\varphi_k^{(i)}\right\}_{i=1}^{2}$	The *ideal* features of training data used to check if an eavesdropper is attacking user k. These two features are theoretically formulated.
$\left\{f_k^{(i)}[t]\right\}_{i=1}^{3}$	The practical features of the t-th training sample in training data. These three features are formulated based on post-processing signals.
$\left\{\widehat{f}_k^{(i)}\left[\widehat{t}\,\right]\right\}_{i=1}^{3}$	The features of the $\widehat{t}$-th training sample in ATD.
T	When a certain pilot is requested for authentication during uplink phase, it is repeatedly sent T times.
$\widehat{T}$	The number of *artificial* training samples that are stuck with the label (#1) (or the label (#0)).
T_{tot}	The total number of training samples that are fed into SVM algorithms. In numerical results, $T_{tot} = 2\widehat{T}$.
(#1), $\mathcal{H}_1$	There is an eavesdropping attack.
(#0), $\mathcal{H}_0$	There is not any eavesdropping attack.

Notations: $\text{sign}(z) = 1$ if $z > 0$ and $\text{sign}(z) = -1$ if $z \leq 0$. Vectors and matrices are represented with lowercase boldface and uppercase boldface, respectively. $[\cdot]^T$ and $[\cdot]^\dagger$ denote the transpose operator, and Hermitian operator, respectively. $\mathbf{I}_L$ is the $L \times L$ identity matrix. $\|\cdot\|$ denotes the Euclidean norm. $\mathbf{z} \sim \mathcal{CN}(\mathbf{0}, \mathbf{I}_L)$ denotes a complex Gaussian random vector $\mathbf{z} \in \mathbb{C}^{L\times 1}$ with zero-mean and covariance $\mathbf{I}_L$. $\mathbb{E}_{\mathbf{v}_1,\ldots,\mathbf{v}_M}\{\cdot\}$ denotes expectation over some variables $\mathbf{v}_1, \ldots, \mathbf{v}_M$. Some important symbols are defined in Table I, while the remaining symbols will be defined whenever used.

II. A Brief Introduction to SVM and OC-SVM

A. The Development of Typical Models

In the 1960s, the perceptron was suggested using the functional relation $l = \text{sign}(\langle \mathbf{w}, \mathbf{r}\rangle + b)$ between the input vector $\mathbf{r} \in \mathcal{R} \subseteq \mathbb{C}^{n\times 1}$ and the output value l. Herein, l is referred to as the label for the input vector $\mathbf{r}$ and yet, assigning a

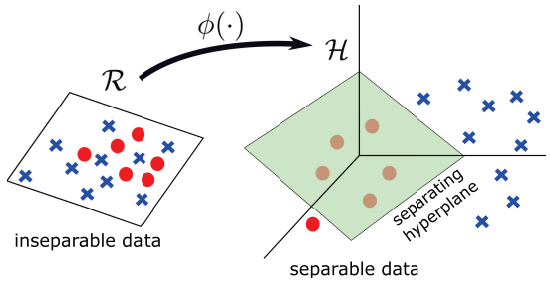

Fig. 1. Using kernel methods, the data in the input space can become more linearly separable in a higher-dimensional space.

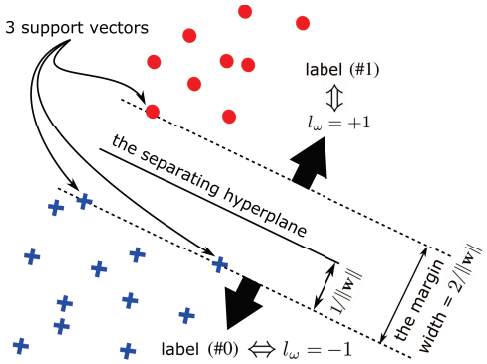

Fig. 2. A dataset, with two types of samples, is separated by a separating hyperplane. The ω-th sample, which is positioned at $\mathbf{x}_\omega$, will be labelled as $(\#1)$ (or $l_w = +1$) if it lies above the separating hyperplane. Otherwise, it will be labelled as $(\#0)$ (or $l_w = -1$).

value (either 1 or -1) to l implies the classification of the input vector. For example, if $l = 1$ means that $\mathbf{r}$ has some attribute A, then $l = -1$ can be used to show that $\mathbf{r}$ is not of that attribute A. Due to the above-mentioned functional relation, the input space $\mathcal{R}$ is separated into two regions by the hyperplane $\langle \mathbf{w}, \mathbf{r} \rangle - b = 0$. In a region, l can take the value 1. In the other region, the value of l is (-1). Given that the binary classification depends on the position of the separating hyperplane, during the learning process the perceptron seeks the most suitable coefficients $\mathbf{w}$ and b such that assigning a value to l (i.e. classifying $\mathbf{r}$) is as optimal as possible.

By replacing $\text{sign}(\cdot)$ with the continuous sigmoid functions, such as $\tanh(\cdot)$, *multi-layer perceptrons* (MLPs) were formed. Among other classifiers are support vector machines (SVMs) that provide better results than the classical MLPs in many cases [17]–[19]. Various SVM classifiers are constructed based on different types of kernel functions, such as the *radial basis function* (RBF) kernel and the sigmoid kernel. The role of kernel functions are significant in terms of calculation and execution time. Moreover, the advantages of SVM classifiers include the ability to work well on small data sets.

B. Kernel Methods

Prior to describing the working mechanism of SVMs, we will clarify the role of kernel functions in SVM classifiers. Let $\phi(\cdot) : \mathcal{R} \rightarrow \mathcal{H}$ be a nonlinear mapping that stretches the *input space* $\mathcal{R}$ to a higher-dimensional space $\mathcal{H}$ (the *feature space*). If $\mathbf{x}_t \in \mathcal{R}$ and $\mathbf{x}_{t'} \in \mathcal{R}$, then the inner product $\mathcal{K}(\mathbf{x}_t, \mathbf{x}_{t'}) = \langle \phi(\mathbf{x}_t), \phi(\mathbf{x}_{t'}) \rangle$ is a kernel function [20], [21]. The main rationale for using the kernel function is that once it has been given beforehand, one can directly compute $\mathcal{K}(\mathbf{x}_t, \mathbf{x}_{t'})$ from $\mathbf{x}_t$ and $\mathbf{x}_{t'}$ without necessarily having explicit expressions for $\phi(\mathbf{x}_t)$ and $\phi(\mathbf{x}_{t'})$ during learning. That helps to accelerate the computational speed. Moreover, the kernel function allows us to avoid working in $\mathcal{R}$; instead, we only evaluate the input samples using the inner product in $\mathcal{H}$. From the viewpoint of data classification, the map $\phi(\cdot)$ can help to convert *linearly inseparable* data (in $\mathcal{R}$) into the data with linearly separable structures (in $\mathcal{H}$) [21]. As an example, Figure 1 illustrates the reason for mapping data points in $\mathcal{R}$ to the associated data points $\mathcal{H}$.

C. Classification based on Classical SVM

The binary classification problem based on SVM can be formulated as follows [21], [22]:

$$\min_{\mathbf{w},b} \quad \frac{1}{2}\|\mathbf{w}\|^2 \tag{1a}$$

$$\text{s.t.} \quad l_\omega \left(\langle \mathbf{w}, \mathbf{x}_\omega \rangle + b \right) \geq 1 \tag{1b}$$

where $\mathbf{x}_\omega$ is the position vector of the ω-th sample, $\omega \in \Omega \triangleq \{1, 2, \ldots, T_{tot}\}$, and T_{tot} is the total number of training samples. $l_\omega = +1$ if $\mathbf{x}_\omega$ is labelled as (#1); otherwise, $l_\omega = -1$ if $\mathbf{x}_\omega$ is labelled as (#0).

As illustrated in Figure 2, the samples are separated by a separating hyperplane that takes the form of $h(\mathbf{x}) = \langle \mathbf{w}, \mathbf{x} \rangle + b = 0$. The separating hyperplane is in the middle of two margins, and the Euclidean distance between the two margins is equal to $2/\|\mathbf{w}\|$. The goal of (1) is to maximize the margin width $2/\|\mathbf{w}\|$, such that the samples are correctly separated. Note that the maximizing $2/\|\mathbf{w}\|$ is equivalent to (1a), while the correct separation is equivalent to (1b).

Let $\Omega_{(\#0)}$ and $\Omega_{(\#1)}$ denote the set of indices $\{\omega \in \Omega | l_\omega = -1\}$ and the set of indices $\{\omega \in \Omega | l_\omega = 1\}$, respectively. If (1) has optimal solutions $\mathbf{w} = \mathbf{w}_\star$ and $b = b_\star$, then we say that $\mathcal{X} = \{(\mathbf{x}_\omega, l_\omega) \, | \omega \in \Omega\}$ are *linearly separable*. In this case, there exists at least one separating hyperplane that separates the samples into two sub-sets, i.e., $\mathcal{X}_{(\#0)} = \{(\mathbf{x}_\omega, l_\omega) \, | \omega \in \Omega_{(\#0)}\}$ and $\mathcal{X}_{(\#1)} = \mathcal{X} \setminus \mathcal{X}_{(\#0)}$. Furthermore, the optimal separating hyperplane among possibly separating hyperplanes will have the following equation:

$$h_\star(\mathbf{x}) = \langle \mathbf{w}_\star, \mathbf{x} \rangle + b_\star = 0. \tag{2}$$

Note that $\mathbf{x}$ in (2) is not necessarily the same as $\mathbf{x}_\omega$ ($\omega \in \Omega$). A certain labelled sample $\mathbf{x}_\omega$ ($\omega \in \Omega$) only lies on the optimal hyperplane if it satisfies $h_\star(\mathbf{x}_t) = 0$. Through the hyperplane $h_\star(\mathbf{x})$, the input space is divided into two sub-spaces. While one sub-space contains all samples $\mathbf{x}_\omega \in \mathcal{X}_{(\#0)}$, the other sub-space contains all samples $\mathbf{x}_\omega \in \mathcal{X}_{(\#1)}$.

It should be noted that (1) may not work in numerous practical scenarios because the labelled samples are linearly inseparable. In this case, classification tasks simply fail to work and no hyperplane can be found. For this reason, the

use of kernel methods will make classification tasks become easier when inseparable data can be translated into the feature space in which the structure of data becomes more separable [20]–[22].[1] Thus, we will replace $\mathbf{x}_\omega$ in (1) with the function $\phi(\mathbf{x}_\omega)$ so as to avoid working directly in the input space. A problem is that the transformed data may remain inseparable. To overcome this difficulty, slack variables $\xi_\omega \geq 0$ are added to the classification problems (see [23] and [24, ch.7]). This breakthrough method has become the background of SVM-based classification methods [23]. Following this method, one can change the original problem (1) over to the following:

$$\min_{\mathbf{w},b,\xi_t} \quad \underbrace{\frac{1}{2}\|\mathbf{w}\|^2}_{\text{regularizer}} + \underbrace{C\sum_{\omega=1}^{T_{tot}}\xi_\omega}_{\text{error}} \tag{3a}$$

$$\text{s.t.} \quad l_\omega\left(\langle \mathbf{w}, \phi\left(\mathbf{x}_\omega\right)\rangle + b\right) \geq 1 - \xi_\omega \tag{3b}$$

where C is the regularization/margin parameter. (3) is called a $L1$ soft-margin SVM. If $\xi_\omega = 0$ for $\forall \omega \in \Omega$, then (3) reduces to the hard-margin SVM (1). Otherwise, with $\xi_\omega \neq 0$, we accept that the ω-th sample $\mathbf{x}_\omega$ can be misclassified [20, Ch.2]. In literature, (3) is transformed into an equivalent optimization problem through the use of Lagrangian function and Karush–Kuhn–Tucker conditions [20], i.e.,

$$\max_{a_1,\ldots,a_T} \quad \sum_{\omega=1}^{T_{tot}} a_\omega - \frac{1}{2}\sum_{\substack{\omega=1\\ \omega'=1}}^{T_{tot}} a_\omega a_{\omega'} l_\omega l_{\omega'} \mathcal{K}\left(\mathbf{x}_\omega, \mathbf{x}_{\omega'}\right) \tag{4a}$$

$$\text{s.t.} \quad \sum_{\omega=1}^{T} a_\omega l_\omega = 0 \tag{4b}$$

$$0 \leq \alpha_\omega \leq C, \ \omega \in \Omega \tag{4c}$$

where $\mathcal{K}\left(\mathbf{x}_\omega, \mathbf{x}_{\omega'}\right) \triangleq \langle \phi(\mathbf{x}_\omega), \phi(\mathbf{x}_{\omega'})\rangle$ is the kernel function.

Remark 1. *Any data point for which $a_\omega = 0$ will not contribute to predictions for new data points, thus only the data points for which $a_\omega \neq 0$ are called SVs. Any data point for which $0 < a_\omega < C$ is called an unbounded SV. Also, any data point for which $a_\omega = C$ is called a bounded SV. While the unbounded SVs lie on the margins, the bounded SVs are between the two margins (see [20, p.24]). In addition, we denote $\mathcal{S}$ as the set of indices of all SVs, $\mathcal{U}$ as the set of unbounded SV indices, and $\mathcal{S} \setminus \mathcal{U}$ as the set of bounded SV indices. Note that $\mathcal{U} \subseteq \mathcal{S} \subseteq \Omega$.*

The equation of the optimal hyperplane is given by

$$h_{(\star|\text{SVM})}(\mathbf{x}) = \sum_{s\in S} a_s l_s \mathcal{K}\left(\mathbf{x}_s, \mathbf{x}\right) + b \tag{5}$$

where b is calculated for unbounded SVs (see [20, ch.2] or [24, (7.37)])

$$b = \frac{1}{|U|}\sum_{u\in U}\left(l_u - \sum_{s\in S} a_s l_s \mathcal{K}\left(\mathbf{x}_s, \mathbf{x}_u\right)\right). \tag{6}$$

Note that in (5)–(6), $\mathbf{x}_s$ is the s-th SV. Meanwhile, $\mathbf{x}_u$ is the u-th unbounded SV. Due to $\mathcal{U} \subseteq \mathcal{S}$, we have the fact $\{\mathbf{x}_u | u \in \mathcal{U}\} \subseteq \{\mathbf{x}_s | s \in \mathcal{S}\}$. For the kernel $\mathcal{K}\left(\mathbf{x}_s, \mathbf{x}\right)$, we will consider four specific functions in Section V for comparison purposes.

[1]Once again, Figure 1 illustrates the role of kernel methods in translating inseparable data points in the two-dimensional space into separable data points in the three-dimensional space.

D. Classification based on OC-SVM

Slightly different from classical SVM models, an OC-SVM model is described as follows [25]–[27]:

$$\underset{\mathbf{w},\rho,\xi_i}{\text{minimize}} \quad \underbrace{\frac{1}{2}\|\mathbf{w}\|^2}_{\text{regularizer}} + \underbrace{\frac{1}{\nu T_{tot}}\sum_{w=1}^{T_{tot}}\xi_w - \rho}_{\text{error}} \tag{7a}$$

$$\text{subject to} \quad \langle \mathbf{w}, \phi(\mathbf{x}_w)\rangle \geq \rho - \xi_w. \tag{7b}$$

Herein, ρ is an offset parameter determining the distance from the origin to the hyperplane, $\nu \in (0, 1]$ is a parameter balancing the maximal distance from the origin and the number of data points in the region created by the hyperplane [26]. Each $\xi_w \geq 0$ is a slack variable, and $\phi(\cdot) : \mathcal{X} \to \mathcal{F}$ is a mapping that tretches the input space $\mathcal{X}$ to a higher-dimensional space $\mathcal{F}$ (namely, the feature space). Once this minimization problem has been solved, the decision function will be given by

$$y(\mathbf{x}) = \text{sign}\left(\mathbf{w}^T\phi(\mathbf{x}) - \rho\right). \tag{8}$$

According to [27], most of the data points are put into a region (e.g., a ball) and these data points in the set $\{\mathbf{x}_1, \ldots, \mathbf{x}_{T_{tot}}\}$ will be labelled $+1$. At the same time, any data point outside the region will be referred to as *outliers*. Consequently, some true outliers might be possibly misclassified when being put inside the region. In short, the use of OC-SVMs is to create a region for most of the data points in $\mathcal{X}$. While the remaining ones lie outside the region and are considered as being associated with eavesdropping attacks.

III. Collecting Wireless Signals and Creating/Defining Features

While the previous section presents useful tools for classifying new data, this section shows the process of creating relevant features and then forming datasets.

A. Collecting Wireless Data

We consider a system with one access point (AP) and K users in the presence of an active eavesdropper (Eve). Each node is equipped with a single antenna and all nodes are randomly positioned. Let the channel between the AP and the k-th user be g_k. Similarly, the channel between the AP and Eve is denoted by g_{E}. The transmission includes 2 phases: Uplink phase for authentication and downlink phase for confidential data transmission.

1) Uplink Phase: For the purposes of authentication and channel estimation, the AP requests legal users to send pilot vectors before it transmits confidential messages in return. The k-th user (or user k) is assumed to send some pilot vector $\mathbf{p}_k$ to the AP. Herein, $\mathbf{p}_k \in \mathbb{C}^{\mathcal{L}\times 1}$ is a column vector with $\mathcal{L}$ entries. By assuming $\mathcal{L} \geq K$, we can design K orthogonal pilot vectors such that $\mathbf{p}_k^\dagger \mathbf{p}_{k'} = 0$ for $k \neq k'$ and $\|\mathbf{p}_k\|^2 = 1$. If Eve wants to overhear the signal s_k that is intended for the

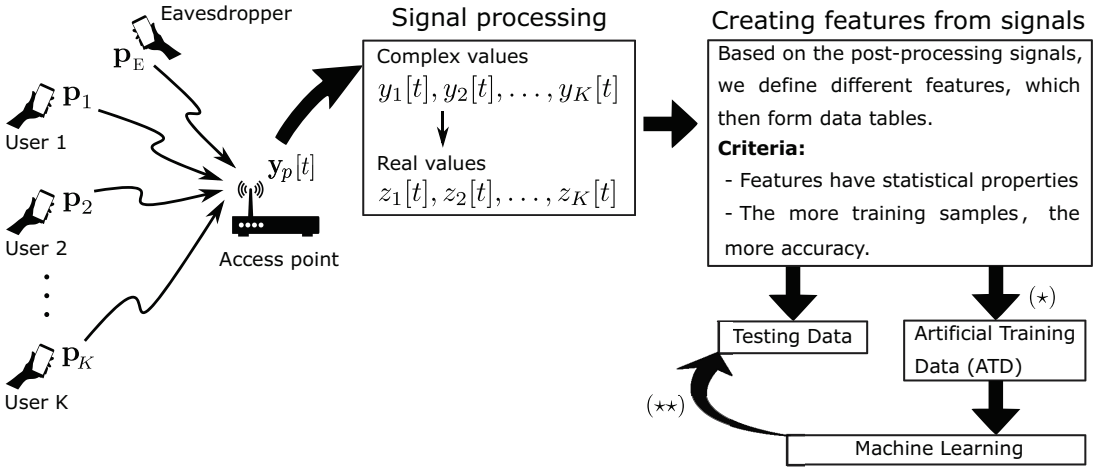

Fig. 3. System model. At the stage $(\star)$, the AP forms the ATD by imitating the uplink phase and simulating signal processing. Using machine learning algorithms, the AP has the trained models and uses them for predicting the testing data at the stage $(\star\star)$.

k-th user, Eve will design her pilot sequence $\mathbf{p}_{\mathrm{E}}$ as the same as $\mathbf{p}_k$ and will send $\mathbf{p}_{\mathrm{E}}$ to the AP (see [5] and [28]). After receiving pilots from legal users and Eve, the AP considers these pilot as the requests for information. Consequently, in the downlink, the AP will send the confidential signal s_k, which is intended for user k, to both user k and Eve. That causes the secret information between the AP and the k-th user to be leaked to Eve.

At some instance t, the AP receives the following signal

$$\mathbf{y}_p[t] = \begin{cases} \sqrt{\mathcal{L}\rho_u}\sum_{k=1}^{K}\mathbf{p}_k g_k[t] + \mathbf{n}[t], & \text{non-attack} \\ \sqrt{\mathcal{L}\rho_u}\sum_{k=1}^{K}\mathbf{p}_k g_k[t] + \sqrt{\mathcal{L}\rho_{\mathrm{E}}}\mathbf{p}_{\mathrm{E}} g_{\mathrm{E}}[t] & \\ \qquad\qquad + \mathbf{n}[t], & \text{attack} \end{cases}. \quad (9)$$

where $\rho_u \triangleq P_u/N_0$ and $\rho_{\mathrm{E}} \triangleq P_{\mathrm{E}}/N_0$. Herein, P_u and P_{E} are the average transmit power of each user and that of Eve, respectively; while N_0 is the average noise power per a receive antenna. $\mathbf{n}$ is an additive white Gaussian noise (AWGN) vector with $\mathbf{n} \sim \mathcal{CN}(\mathbf{0}, \mathbf{I}_{\mathcal{L}})$. Note that $\mathbf{y}_p[t]$, $g_k[t]$, $g_{\mathrm{E}}[t]$ and $\mathbf{n}[t]$ are the realizations of $\mathbf{y}_p$, g_k, g_{E} and $\mathbf{n}$ at time t, respectively.

2) Downlink Phase: In the downlink phase, the AP transmits signals to legal users. Of course, Eve also receives the signals intended for user k because the AP assumes that two legal users (i.e., user k and Eve) are requesting the same messages. Recall that the AP may not be aware of the presence of Eve and her attacks.

It is shown that the data rate of user k reduces when Eve breaks into the uplink phase (see [5] for more details). In other words, the signal-to-noise ratio (SNR) of the k-th user, denoted as snr_k, reduces with the increase in Eve's power. Consequently, the difference between the data rate of user k and the data rate of Eve, namely the security rate, also becomes lower.

As such, it is crucial that we must be able to detect the presence of Eve in the uplink phase. Once the AP has identified an eavesdropping attack, it will be able to design suitable strategies, such as the use of beamforming and artificial noise, to deal with Eve. Herein, we do not delve into such strategies in the downlink phase because this topic is plentiful in the literature (see [5] and references therein). Instead, the SVM-based methods of detecting active eavesdropping attacks in the uplink phase will be considered only.

B. Creating Features/Attributes

By projecting $\mathbf{y}_p[t]$ along the pilot vector $\mathbf{p}_k^{\dagger}$, we have the post-processing signal $y_k[t] = \mathbf{p}_k^{\dagger}\mathbf{y}_p[t]$, i.e.

$$y_k[t] = \begin{cases} \sqrt{\mathcal{L}\rho_u} g_k[t] + \mathbf{p}_k^{\dagger}\mathbf{n}[t], & \text{non-attack} \\ \sqrt{\mathcal{L}\rho_u} g_k[t] + \sqrt{\mathcal{L}\rho_{\mathrm{E}}} g_{\mathrm{E}}[t] + \mathbf{p}_k^{\dagger}\mathbf{n}[t], & \text{attack} \end{cases}. \quad (10)$$

Proceeding with defining $z_k[t] \triangleq |y_k[t]|^2$, the AP can calculate

$$\varphi_k^{(1)} \triangleq \mathbb{E}_t\left\{z_k[t]\right\}, \quad (11)$$

$$\varphi_k^{(2)} \triangleq \frac{\mathbb{E}_t\left\{z_k[t]\right\} - \mathbb{E}_t\left\{\left|\mathbf{p}_k^{\dagger}\mathbf{n}[t]\right|^2\right\}}{\mathbb{E}_t\left\{\left|\mathbf{p}_k^{\dagger}\mathbf{n}[t]\right|^2\right\}} \quad (12)$$

based on the sufficiently statistical knowledge of $\{g_k\}_{k=1}^K$ and g_{E}. Note that $\mathbb{E}_t\{\cdot\} \equiv \mathbb{E}_{\{g_k\}_{k=1}^K, g_{\mathrm{E}}, \mathbf{n}}\{\cdot\}$ due to the dependence of $\{g_k\}_{k=1}^K$, g_{E} and $\mathbf{n}$ on t.

In practice, if user k sends its pilot vector $\mathbf{p}_k$ to the AP T times,[2] then the AP will have T different values $z_k[1]$, $\ldots$, $z_k[T]$. Using these values, the AP will make a structured dataset that consists of the following two features:

- Feature 1 (MEAN):

$$f_k^{(1)}[T] \triangleq \frac{1}{T}\sum_{t=1}^{T} z_k[t] = \begin{cases} f_{k|\mathcal{H}_0}^{(1)}[T], & \text{non-attack} \\ f_{k|\mathcal{H}_1}^{(1)}[T], & \text{attack} \end{cases}. \quad (13)$$

Herein, $\mathcal{H}_0$ implies that there is not any eavesdropping attack. Meanwhile, $\mathcal{H}_0$ implies an eavesdropping attack.

[2]Herein, $\mathbf{p}_k$ is repeatedly sent for authentication.

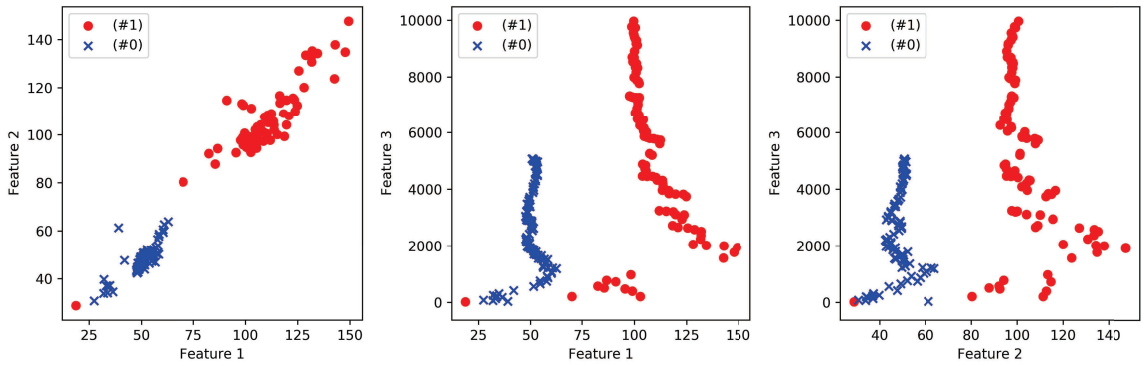

Fig. 4. An illustration of the data points in the ATD before normalization. The red circles are labelled as (#1), while the cross markers are labelled as (#0).

- Feature 2 (RATIO):

$$f_k^{(2)}[T] \triangleq \frac{\sum_{t=1}^{T} z_k[t] - \sum_{t=1}^{T} |\mathbf{p}_k^{\dagger}\mathbf{n}[t]|^2}{\sum_{t=1}^{T} |\mathbf{p}_k^{\dagger}\mathbf{n}[t]|^2} = \begin{cases} f_{k|\mathcal{H}_0}^{(2)}[T], & \text{non-attack} \\ f_{k|\mathcal{H}_1}^{(2)}[T], & \text{attack} \end{cases}. \tag{14}$$

Statistically, if the AP receives the sufficient number of samples (i.e., if T is large enough), we can reach

$$f_k^{(1)}[T] \overset{\text{large } T}{\approx} \varphi_k^{(1)}, \tag{15}$$

$$f_k^{(2)}[T] \overset{\text{large } T}{\approx} \varphi_k^{(2)}. \tag{16}$$

The AP can request that the pilot vector $\mathbf{p}_k$ has to be sent T times by user k for the purpose of threat detection. In doing that, the AP will have $\{z_k[1], \ldots, z_k[T]\}_{k=1}^{K}$. From this sequence, we can calculate the sum

$$\sum_{t=1}^{T} z_k[t] = T f_k^{(1)}[T] \overset{\text{large } T}{\approx} T\varphi_k^{(1)} \tag{17}$$

using (13) and (15). In the case of an eavesdropping attack, the sum is equal to $T f_{k|\mathcal{H}_1}^{(1)}[T]$. Otherwise, the sum is equal to $T f_{k|\mathcal{H}_0}^{(1)}[T]$. Herein, the absolute difference between the two cases is $T\left|f_{k|\mathcal{H}_1}^{(1)}[T] - f_{k|\mathcal{H}_0}^{(1)}[T]\right|$, which increases with T. Obviously, the larger T, the larger difference. Based on what has just been observed, we suggest creating another feature that relates to the sum of $\{z_k[1], \ldots, z_k[T]\}$ as follows:

- Feature 3 (SUM):

$$f_k^{(3)}[T] \triangleq \sum_{t=1}^{T} z_k[t] = \begin{cases} f_{k|\mathcal{H}_0}^{(3)}[T], & \text{non-attack} \\ f_{k|\mathcal{H}_1}^{(3)}[T], & \text{attack} \end{cases}. \tag{18}$$

Remark 2. *The features 1 and 3, i.e., MEAN and SUM, are not exactly the same, although* (13) *can be calculated from* (18) *or vice versus. The difference lies in that when T is large enough, $f_k^{(1)}[T]$ will converge to a certain constant $\varphi_k^{(1)}$, but $f_k^{(3)}[T]$ will tend to increase its value. In other words, with a very large value of T, $f_k^{(1)}[T]$ will be independent of T, while $f_k^{(3)}[T]$ will be linearly dependent on T. Intuitively, the third feature is expected to make data more separable than the first feature. However, it seems to be impractical to take a very large value of T, because the AP should not request users to send pilot sequences too many times for authentication. Thus, it is questionable whether SUM is really a more desirable feature than MEAN in terms of implementation, with a limited value of T. In Subsection V-A, this concern will be clarified.*

TABLE II
TESTING DATA: T POINTS ARE ASSOCIATED WITH THE LABEL (#0) AND T POINTS ARE ASSOCIATED WITH THE LABEL (#1).

Fearture 1 (MEAN)	Fearture 2 (RATIO)	Fearture 3 (SUM)
$f_{k\|\mathcal{H}_0}^{(1)}[1]$	$f_{k\|\mathcal{H}_0}^{(2)}[1]$	$f_{k\|\mathcal{H}_0}^{(3)}[1]$
$\vdots$	$\vdots$	$\vdots$
$f_{k\|\mathcal{H}_0}^{(1)}[T]$	$f_{k\|\mathcal{H}_0}^{(2)}[T]$	$f_{k\|\mathcal{H}_0}^{(T)}[T]$
$f_{k\|\mathcal{H}_1}^{(1)}[1]$	$f_{k\|\mathcal{H}_1}^{(2)}[1]$	$f_{k\|\mathcal{H}_1}^{(3)}[1]$
$\vdots$	$\vdots$	$\vdots$
$f_{k\|\mathcal{H}_0}^{(1)}[T]$	$f_{k\|\mathcal{H}_0}^{(2)}[T]$	$f_{k\|\mathcal{H}_0}^{(T)}[T]$

In short, we can create a testing dataset from wireless signals. Table II illustrates the three features of the testing data used in this paper, and Figure 4 illustrates the data points of an ATD in two-dimensional domains. The position of the t-th data point in the 3-dimensional space is $(f_k^{(1)}[t], f_k^{(2)}[t], f_k^{(3)}[t])$. Note that the subscript k still implies that we are checking if the k-th user is under attack. It should also be noted that our testing data has not yet been labelled. In Figure 5, the impact of T on the distribution of data points is shown. It can be seen that the first data points are close together and hard to be separated. However, the larger T, the more separable the data becomes.

IV. ARTIFICIAL TRAINING DATA (ATD)

In this section, artificial training data (ATD) will be created. The ATD used for SVM corresponds to the case of having both the legal users' CSI and the eavesdropper's CSI. Meanwhile, the ATD used for OC-SVM corresponds to the case of having only the legal users' CSI.

A. ATD for (Classical) SVM

The access point can create the ATD by imitating the uplink phase. More specifically, we perform the following steps:

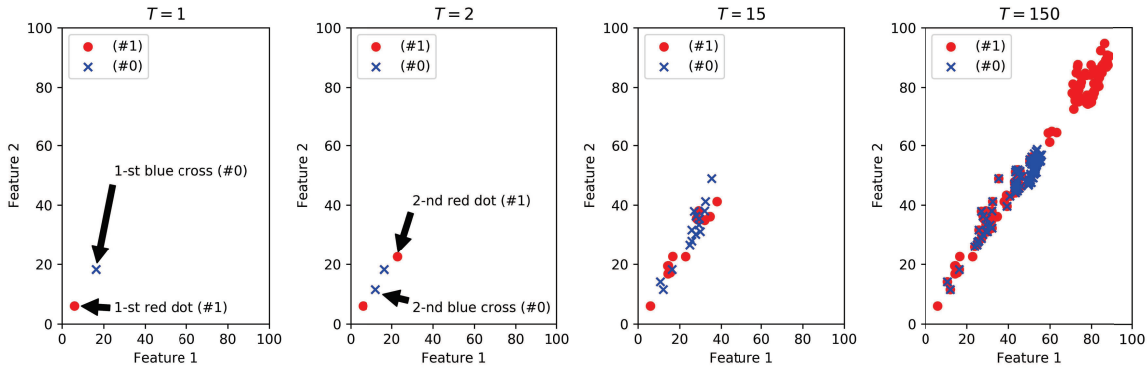

Fig. 5. The distribution of data points in $\mathbb{R}^2$. The 1-st red dot and the 1-st blue cross are, respectively, positioned at $\left(f^{(1)}_{k|\mathcal{H}_1}[1], f^{(2)}_{k|\mathcal{H}_1}[1]\right)$ and at $\left(f^{(1)}_{k|\mathcal{H}_0}[1], f^{(2)}_{k|\mathcal{H}_0}[1]\right)$. Similarly, the 2-nd red dot and the 2-nd blue cross are, respectively, positioned at $\left(f^{(1)}_{k|\mathcal{H}_1}[2], f^{(2)}_{k|\mathcal{H}_1}[2]\right)$ and at $\left(f^{(1)}_{k|\mathcal{H}_0}[2], f^{(2)}_{k|\mathcal{H}_0}[2]\right)$. When the value of T increases, red dots tend to cluster together and become separable from blue crosses.

- Step 1: Start with $k = 1$.
- Step 2: Start with $\widehat{t} = 1$.
- Step 3: Generate $\widehat{g}_k \overset{dist}{=} g_k$, $\widehat{g}_{\mathrm{E}} \overset{dist}{=} g_{\mathrm{E}}$ and $\widehat{\mathbf{n}} \sim \mathcal{CN}(\mathbf{0}, \mathbf{I}_{\mathcal{L}})$. Note that the notation $X \overset{dist}{=} Y$ implies that X and Y have the same distribution.
- Step 4: Calculate

$$\widehat{z}_k\left[\widehat{t}\,\right] = \begin{cases} \left|\sqrt{\mathcal{L}\rho_u}\widehat{g}_k\left[\widehat{t}\,\right] + \mathbf{p}_k^{\dagger}\widehat{\mathbf{n}}\left[\widehat{t}\,\right]\right|^2, & \text{non-attack} \\ \left|\sqrt{\mathcal{L}\rho_u}\widehat{g}_k\left[\widehat{t}\,\right] + \sqrt{\mathcal{L}\rho_{\mathrm{E}}}\widehat{g}_{\mathrm{E}}\left[\widehat{t}\,\right] + \mathbf{p}_k^{\dagger}\widehat{\mathbf{n}}\left[\widehat{t}\,\right]\right|^2, & \text{attack} \end{cases} \tag{19}$$

$$\widehat{f}^{(1)}_k\left[\widehat{t}\,\right] = \frac{1}{\widehat{t}}\sum_{\varsigma=1}^{\widehat{t}}\widehat{z}_k[\varsigma] = \begin{cases} \widehat{f}^{(1)}_{k|\mathcal{H}_0}\left[\widehat{t}\,\right], & \text{non-attack} \\ \widehat{f}^{(1)}_{k|\mathcal{H}_1}\left[\widehat{t}\,\right], & \text{attack} \end{cases}, \tag{20}$$

$$\widehat{f}^{(2)}_k\left[\widehat{t}\,\right] = \frac{\sum_{\varsigma=1}^{\widehat{t}}\widehat{z}_k[\varsigma] - \sum_{\varsigma=1}^{\widehat{t}}|\mathbf{p}_k^{\dagger}\widehat{\mathbf{n}}[\varsigma]|^2}{\sum_{\varsigma=1}^{\widehat{t}}|\mathbf{p}_k^{\dagger}\widehat{\mathbf{n}}[\varsigma]|^2} = \begin{cases} \widehat{f}^{(2)}_{k|\mathcal{H}_0}\left[\widehat{t}\,\right], & \text{non-attack} \\ \widehat{f}^{(2)}_{k|\mathcal{H}_1}\left[\widehat{t}\,\right], & \text{attack} \end{cases}, \tag{21}$$

$$\widehat{f}^{(3)}_k\left[\widehat{t}\,\right] = \sum_{\varsigma=1}^{\widehat{t}}\widehat{z}_k[\varsigma] = \begin{cases} \widehat{f}^{(3)}_{k|\mathcal{H}_0}\left[\widehat{t}\,\right], & \text{non-attack} \\ \widehat{f}^{(3)}_{k|\mathcal{H}_1}\left[\widehat{t}\,\right], & \text{attack} \end{cases}. \tag{22}$$

- Step 5: We stick the label (#0) to the $\widehat{t}$-th data point $\left(\widehat{f}^{(1)}_{k|\mathcal{H}_0}\left[\widehat{t}\,\right], \widehat{f}^{(2)}_{k|\mathcal{H}_0}\left[\widehat{t}\,\right], \widehat{f}^{(3)}_{k|\mathcal{H}_0}\left[\widehat{t}\,\right]\right)$ in order to imply that user k is not under an attack. In contrast, we stick the label (#1) to the $\widehat{t}$-th data point $\left(\widehat{f}^{(1)}_{k|\mathcal{H}_1}\left[\widehat{t}\,\right], \widehat{f}^{(2)}_{k|\mathcal{H}_1}\left[\widehat{t}\,\right], \widehat{f}^{(3)}_{k|\mathcal{H}_1}\left[\widehat{t}\,\right]\right)$ in order to imply that user k is under an attack.
- Step 6: Set $\widehat{t} = \widehat{t}+1$ and repeat Steps 3-5. Go to Step 7 if $\widehat{t} > \widehat{T}$. Herein, $\widehat{T}$ is a large number that can be freely determined by designers. To make the ATD statistically reliable, we choose $\widehat{T} \gg T$.
- Step 7: Set $k = k+1$ and repeat Steps 2-6. Stop the process if $k > K$.

TABLE III
ARTIFICIAL TRAINING DATA (ATD) USED FOR CLASSICAL SVM

MEAN	RATIO	SUM	Labels
$\widehat{f}^{(1)}_{k\|\mathcal{H}_1}[1]$	$\widehat{f}^{(2)}_{k\|\mathcal{H}_1}[1]$	$\widehat{f}^{(3)}_{k\|\mathcal{H}_1}[1]$	(#1)
$\vdots$	$\vdots$	$\vdots$	$\vdots$
$\widehat{f}^{(1)}_{k\|\mathcal{H}_1}[\widehat{T}]$	$\widehat{f}^{(2)}_{k\|\mathcal{H}_1}[\widehat{T}]$	$\widehat{f}^{(3)}_{k\|\mathcal{H}_1}[\widehat{T}]$	(#1)
$\widehat{f}^{(1)}_{k\|\mathcal{H}_0}[1]$	$\widehat{f}^{(2)}_{k\|\mathcal{H}_0}[1]$	$\widehat{f}^{(3)}_{k\|\mathcal{H}_0}[1]$	(#0)
$\vdots$	$\vdots$	$\vdots$	$\vdots$
$\widehat{f}^{(1)}_{k\|\mathcal{H}_0}[\widehat{T}]$	$\widehat{f}^{(2)}_{k\|\mathcal{H}_0}[\widehat{T}]$	$\widehat{f}^{(3)}_{k\|\mathcal{H}_0}[\widehat{T}]$	(#0)

Remark 3. *The ATD for classical SVM is shown in Table III. It will be used to train classical SVM models in this paper (and any other supervised learning models). Those trained models are then applied to the testing dataset in Table II, whereby we can classify if the obtained signal is affected by an active eavesdropper.*

Remark 4. *Different from T, we can let $\widehat{T}$ be a very large number because $\widehat{T}$ belongs to an artificial process. For example, in the uplink phase, the AP can request both user k and Eve to send the same pilot vector $\mathbf{p}_k$ three times (i.e., $T = 3$) but cannot request them to send $\mathbf{p}_k$ so many times (e.g., $T = 1000$). However, for an artificial process at the AP, it allows itself to receive a large number of copies of $\mathbf{p}_k$ as desired. With sufficiently large $\widehat{T}$, we can reach $\widehat{f}^{(1)}_k[\widehat{T}]/\varphi^{(1)}_k \approx 1$, $\widehat{f}^{(2)}_k[\widehat{T}]/\varphi^{(2)}_k \approx 1$, and $\widehat{f}^{(3)}_k[\widehat{T}]/\varphi^{(1)}_k \approx \widehat{T}$.*

B. ATD for OC-SVM

While the ATD used for SVM contains two types of data points (corresponding to two labels), the ATD used for OC-SVM contains only one type of data point (corresponding to one label). Obviously, the ATD used for OC-SVM can be extracted from the ATD used for SVM by removing one label and keeping the other label.

TABLE IV
ARTIFICIAL TRAINING DATA (ATD) USED FOR OC-SVM

MEAN	RATIO	SUM	Labels
$\widehat{f}^{(1)}_{k\|\mathcal{H}_0}[1]$	$\widehat{f}^{(2)}_{k\|\mathcal{H}_0}[1]$	$\widehat{f}^{(3)}_{k\|\mathcal{H}_0}[1]$	(#0)
$\vdots$	$\vdots$	$\vdots$	$\vdots$
$\widehat{f}^{(1)}_{k\|\mathcal{H}_0}[\widehat{T}]$	$\widehat{f}^{(2)}_{k\|\mathcal{H}_0}[\widehat{T}]$	$\widehat{f}^{(3)}_{k\|\mathcal{H}_0}[\widehat{T}]$	(#0)

In practical use cases, OC-SVM is related to the case that we do not have the perfect CSI of Eve. Thus, it is reasonable to suppose that the ATD used for OC-SVM only includes data points associated with the label (#0) (i.e., non-attack). Obviously, if we only have the perfect CSI of legal users, we can only simulate the virtual process of transmitting signals from users to Alice and create (#0)-related data points.

Table IV, which is made of the last $\widehat{T}$ rows of Table III, shows the ATD used for OC-SVM. Obviously, Table IV does not include any data points associated with eavesdropping attacks.

C. ATD Normalization/Whitening

Normally, SVM works with data within the range of $[0, 1]$. Thus, it is necessary for the AP to normalize all features in training datasets. Normalizing (or whitening) makes all values in a feature column fall within $[0, 1]$. More specifically, if a certain feature column consists of values $u_1, u_2, \ldots$, and $u_{T_{tot}}$, then the AP will need to run the following algorithm:

- Step 1: Find $u_{min} = \min\{u_1, u_2, \ldots, u_{T_{tot}}\}$ and $u_{max} = \max\{u_1, u_2, \ldots, u_{T_{tot}}\}$.
- Step 2: Compute $u_k^{temp} = \dfrac{u_k - u_{min}}{u_{max} - u_{min}}$ where $k \in \{1, 2, \ldots, T_{tot}\}$. Assign the temporary value u_k^{temp} to u_k by letting $u_k = u_k^{temp}$.

Applying the above algorithm to all feature columns in the ATD, we can normalize the ATD before actually using SVM classifiers. An important note is that if training data (i.e., the ATD in this paper) is normalized, then testing data must also be normalized accordingly.

V. NUMERICAL RESULTS

In this section, we present several numerical examples to evaluate the proposed framework under specific settings. As for the channel fading, we set up $g_k = \sqrt{\beta_k} h_k$ and $g_{\mathrm{E}} = \sqrt{\beta_{\mathrm{E}}} h_{\mathrm{E}}$. Herein, β_k and β_{E} represent the large scale fading, while $h_k \sim \mathcal{CN}(0, 1)$ and $h_{\mathrm{E}} \sim \mathcal{CN}(0, 1)$ represent the small scale fading.[3]

The time complexity depends heavily on the loss function and the optimization method [29]. Using the big-O notation, it is experimentally confirmed that if the implementation is based on LIBSVM, the time complexity of SVM as well as OC-SVM can be about $\mathcal{O}(\widehat{T}_{tot}^3)$ where $\widehat{T}_{tot}$ is the total number of training samples in the ATD [30]–[32]. Our experiments are executed in Python and the execution of each SVM/OC-SVM classifier takes around 0.09 seconds for training an ATD-based model and labelling data points in the testing data.

A. Examining $\widehat{T}$, T, and 3 defined features

Table V compares the accuracy of RBF-based SVM (and OC-SVM) classifiers in 4 different sub-cases:

- i) The input data, which is trained by SVM (and OC-SVM) classifiers, only includes the 1-st feature column, the 2-nd feature column, and the label column in Table III. It means that we only classify data based on the features MEAN and RATIO.
- ii) The input data includes the features MEAN and SUM.
- iii) The input data includes the features RATIO and SUM.
- iv) The input data is exactly the same as Table III that contains all the three defined features, i.e., MEAN, RATIO and SUM.

The results in Table V show that the accuracy increases with T as well as with $\widehat{T}$. The classification has the lowest accuracy when the input data contains only the attributes RATIO and SUM. Noticeably, case i) produces higher accuracy than the whole ATD in some cases. Although SVM offers higher

[3]Although Rayleigh fading is used to model h_k and h_{E}, other types of fading can also be used because the framework, presented in Sections III and IV, is not limited to any specific type of fading.

TABLE V
THE KERNEL FUNCTION, WHICH IS MENTIONED IN (5), IS THE RBF KERNEL, I.E., $\mathcal{K}(\mathbf{x}_s, \mathbf{x}) = \exp\{-\gamma \|\mathbf{x}_s - \mathbf{x}\|\}$. THE SVM PARAMETERS ARE $\gamma = 0.5$ AND $C = 1$. THE OC-SVM PARAMETERS ARE $\nu = 0.02, \gamma = 0.001$. SYSTEM PARAMETERS: $K = 4$, $\mathcal{L} = 10$, $\rho_u = 5$, $\rho_{\mathrm{E}} = 3$, $\beta_k = 1$, $\beta_{\mathrm{E}} = 1$. IN THE TABLE, THE SUB-CASES I), II), III) AND IV) CORRESPOND TO 4 SUB-CASES DESCRIBED IN SUBSECTION V-A.

$\widehat{T}$	T	The accuracy of SVM (%)				The accuracy of OC-SVM (%)			
		i)	ii)	iii)	iv)	i)	ii)	iii)	iv)
100	5	60%	70%	60%	60%	20%	25%	25%	25%
	10	80%	85%	60%	80%	27.5%	50%	50%	50%
	20	**90%**	87.5%	72.5%	**90%**	67.5%	70%	70%	70%
1000	5	80%	80%	60%	60%	22.5%	25%	25%	25%
	10	90%	90%	70%	80%	45%	50%	50%	25%
	20	**95%**	**95%**	77.5%	90%	65%	70%	70%	70%
5000	5	80%	80%	60%	70%	25%	25%	25%	25%
	10	90%	90%	70%	85%	47.5%	50%	50%	50%
	20	**95%**	**95%**	77.5%	92.5%	67.5%	70%	70%	70%

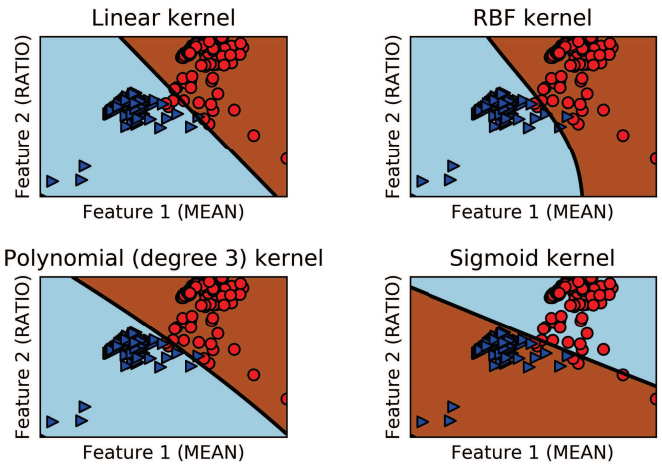

Fig. 6. An illustration of 4 trained SVM models that correspond to four different kernel functions (i.e., linear, RBF, polynomial (degree 3), and sigmoid kernels). The cyan area and ▷ markers relate to (#0), while the brown area and ○ markers relate to (#1).

accuracy than OC-SVM, we have to note that a comparison between these two may be unfair due to the differences inherent in these two approaches (e.g., (3) uses the regularization parameter C, while (7) uses the parameter ν), and that OC-SVM requires only the CSI corresponding the legal users.

There does not seem to be significant difference in accuracy when using datasets with two features (i.e., the sub-cases i, ii and iii) and a dataset with three features (i.e., the sub-case iv). Another observation is that the sub-case i (without the feature SUM) is better than the sub-case iv (with the feature SUM) in the case of SVM. This observation implies that SUM is not as useful as MEAN in terms of implementation. As discussed in Remark 2, the limited value of T might cause our SVM classifiers ineffective as expected.

Thus, we will use the input data, consisting of two features, for training machine learning models in most of the remaining numerical examples.

B. Examining 4 different kernel functions

Table VI shows the accuracy of 4 different SVM (and OC-SVM) classifiers. These classifiers are based on

- linear kernel: $\mathcal{K}(\mathbf{x}_s, \mathbf{x}) = \langle \mathbf{x}_s, \mathbf{x} \rangle$,
- RBF kernel: $\mathcal{K}(\mathbf{x}_s, \mathbf{x}) = \exp\{-\gamma \|\mathbf{x}_s - \mathbf{x}\|\}$,
- polynomial kernel: $\mathcal{K}(\mathbf{x}_s, \mathbf{x}) = (\gamma \langle \mathbf{x}_s, \mathbf{x} \rangle + r)^d$,
- sigmoid kernel: $\mathcal{K}(\mathbf{x}_s, \mathbf{x}) = \tanh(\gamma \langle \mathbf{x}_s, \mathbf{x} \rangle + r)$.

The numerical results in Table VI shows that the RBF kernel brings about the highest accuracy in all considered cases. On the contrary, the sigmoid kernel has the lowest accuracy. Herein, it should also be noted that we set r to 0 such that the RBF, polynomial and sigmoid kernels are fairly treated. In fact, when r and d are set to other values, the RBF kernel might not be the best one any longer.

In need of illustrating the above-mentioned kernel functions, we provide an intuitive comparison in Figure 6. The total number of training samples is $T_{tot} = 2\widehat{T} = 400$, i.e., 200 samples with the label (#1) and 200 samples with the label (#0). SVM parameters: $C = 1$, $\gamma = 5$, and $d = 3$. The system parameters are exactly the same as those used for Table VI. We can see that the separating hyperplane in the case of linear kernel is a straight line, while the three ones are curves. Intuitively comparing all sub-figures, we can state that the fourth sub-case is the worst when the majority of 400 training samples are misclassified. This observation matches what has been recorded in Table VI.

Similarly, Figure 7 illustrates 4 different OC-SVM models with $\widehat{T} = 200, \nu = 0.02$ and $\gamma = 0.001$. We can see that there are only ATD points corresponding to the label (#0) because OC-SVM models are trained on data that has only one class (i.e., one label).

C. Receiver operating characteristic (ROC) curves

According to [33]–[35], true positive rate (or probability of detection) is defined as

$$TPR = \frac{\text{True positive (TP)}}{\text{Positive (Pos)}}$$

where TPR is the number of (#1)-labelled samples that is **correctly** classified as (#1), and Pos is the total number of **actually** (#1)-labelled samples. In contrast, false positive rate (or probability of false alarm) is defined as [35]

$$FPR = \frac{\text{False positive (FP)}}{\text{Negative (Neg)}}$$

where FPR is the number of (#0)-labelled samples that is **wrongly** classified as (#1), and Neg is the total number of **actually** (#0)-labelled samples.

TABLE VI
SVM PARAMETERS: $C = 1, \gamma = 2, r = 0$, AND $d = 3$. OC-SVM PARAMETERS: $\nu = 0.02$ AND $\gamma = 0.001$. THE INPUT DATA INCLUDES THE FEATURES MEAN AND RATIO (I.E., THE FEATURE SUM WILL NOT BE USED). SYSTEM PARAMETERS: $K = 4$, $\mathcal{L} = 10$, $\rho_u = 5$, $\rho_{\text{E}} = 3$, $\beta_k = 1$, $\beta_{\text{E}} = 1$.

$\widehat{T}$	T	The accuracy of SVM (%)				The accuracy of OC-SVM (%)			
		Linear	RBF	Polynomial	Sigmoid	Linear	RBF	Polynomial	Sigmoid
400	5	70%	**80%**	**80%**	40%	17.5%	22.5%	17.5%	17.5%
	10	85%	**90%**	80%	40%	35%	45%	35%	35%
	20	92.5%	**95%**	90%	27.5%	82.5%	95%	82.5%	77.5%
800	5	70%	**80%**	80%	40%	17.5%	22.5%	17.5%	17.5%
	10	85%	**90%**	80%	40%	35%	45%	35%	35%
	20	92.5%	**95%**	90%	27.5%	82.5%	95%	82.5%	77.5%

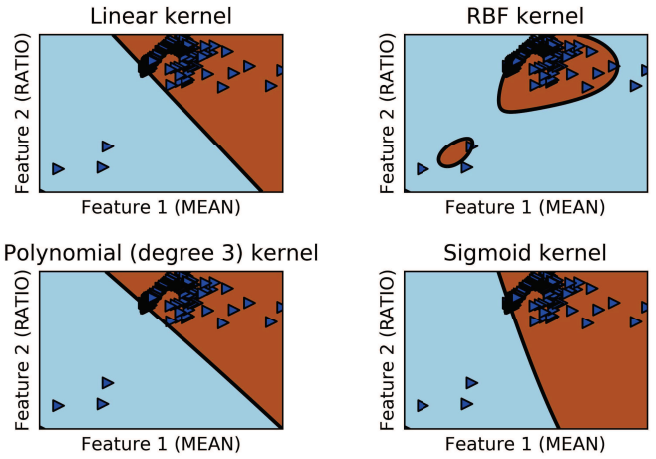

Fig. 7. An illustration of 4 trained OC-SVM models that correspond to linear, RBF, polynomial (degree 3), and sigmoid kernels. ▷ markers are the ATD points associated with the label (#0). The brown area is the area that contains most of the ATD points ▷.

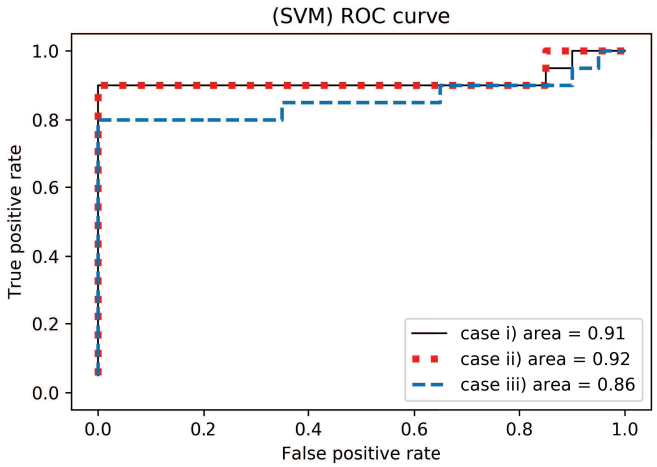

Fig. 8. ROC curves and the areas under corresponding ROC curves in the SVM regime.

To plot the TPR against the FPR in the case of SVM, we offer Figure 8 that contains three receiver operating characteristic (ROC) curves.[4] These ROC curves corresponds to three cases:

- i) the input data includes MEAN and RATIO,

[4]A ROC curve will not applicable for OC-SVM because the training process of an OC-SVM model suffers from a huge imbalance with only one class.

TABLE VII
THE INPUT DATA INCLUDES THE FEATURES MEAN AND RATIO. SVM PARAMETERS: $C = 1$, $r = 0$, AND $d = 3$. OTHER PARAMETERS: $K = 4$, $\mathcal{L} = 10$, $\rho_u = 5$, $\beta_k = 1$, $\beta_{\rm E} = 1$, $(\widehat{T}, T) = (10^4, 15)$.

$\frac{\rho_{\rm E}}{\rho_u}$	γ	The accuracy of SVM (%)			
		Linear	RBF	Polynomial	Sigmoid
0.1	0.05	70%	70%	80%	70%
	0.5	70%	70%	70%	66.67%
	5	70%	66.67%	66.67%	30%
0.5	0.05	86.67%	93.33%	50%	93.33%
	0.5	86.67%	86.67%	76.67%	93.33%
	5	86.67%	80%	86.67%	80%
1	0.05	96.67%	96.67%	80%	96.67%
	0.5	96.67%	96.67%	96.67%	96.6%
	5	96.67%	96.67%	93.33%	3.33%

TABLE VIII
THE INPUT DATA INCLUDES THE FEATURES MEAN AND RATIO. THE OC-SVM PARAMETER ν IS SET TO 0.001. OTHER PARAMETERS: $K = 4$, $\mathcal{L} = 10$, $\rho_u = 5$, $\beta_k = 1$, $\beta_{\rm E} = 1$, $(\widehat{T}, T) = (10^4, 15)$.

$\frac{\rho_{\rm E}}{\rho_u}$	γ	The accuracy of OC-SVM (%)			
		Linear	RBF	Polynomial	Sigmoid
0.1	1	36.67%	50%	36.67%	50%
	10^{-3}	36.67%	50%	36.67%	36.67%
	10^{-6}	36.67%	31.67%	38.33%	38.33%
0.5	1	48.33%	43.33%	48.33%	50%
	10^{-3}	48.33%	40%	48.33%	48.33%
	10^{-6}	48.33%	35%	45%	45%
1	1	50%	50%	50%	50%
	10^{-3}	50%	50%	50%	50%
	10^{-6}	50%	45%	43.33%	43.33%

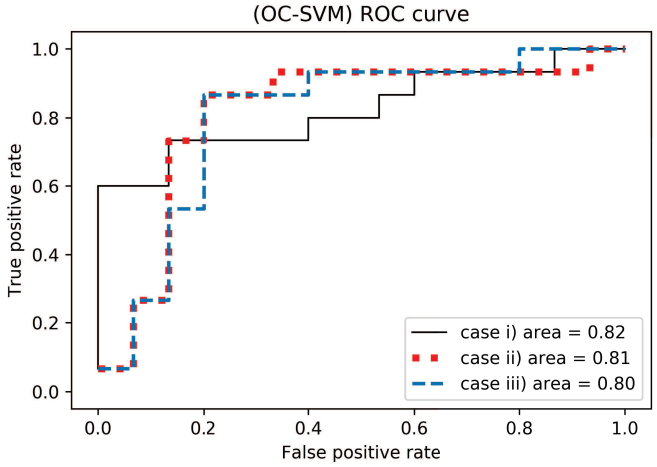

Fig. 9. ROC curves and the areas under corresponding ROC curves in the OC-SVM regime.

- ii) the input data includes MEAN and SUM,
- iii) the input data includes RATIO and SUM.

The parameters used for Figure 8 are as follows: $C = 1$, $\gamma = 0.5$, $\widehat{T} = 5000$, and $T = 20$. Other system parameters remain the same as those in Table VI. The area under the ROC curve (namely, AUC) is 0.91 in case i, 0.92 in case ii, and 0.86 in case iii. As such, case ii is considered as the best case, while case iii is the worst one.

In the case of OC-SVM, we offer Figure 9 to illustrate the ROC curves and AUC values for the three cases i, ii and iii. The parameters used for Figure 9 are as follows: $\nu = 0.02$, $\gamma = 0.001$, $\widehat{T} = 1000$, and $T = 20$. Other system parameters remain the same as those in Table VI. This figure also shows that the case iii is the worst. In addition, the case i is preferred to keep a low FPR and an acceptable TPR (e.g. $FPR \leq 0.2$ and $TPR \approx 0.6$). Whereas, the case ii and iii are better choices to have a higher TPR and an acceptable FPR (e.g., $TPR \geq 0.8$ and $FPR \leq 0.4$).

D. Examining the relation between ρ_E and γ

Table VII and Table VIII show the relationship between the eavesdropper's power and the coefficient γ in the kernel functions. The accuracy, in general, increases with ρ_{E}. For example, the polynomial kernel in Table VII provides the accuracy of 70%, at $\left(\gamma, \frac{\rho_{\mathrm{E}}}{\rho_u}\right) = (0.5, 0.1)$, 76.67% at $\left(\gamma, \frac{\rho_{\mathrm{E}}}{\rho_u}\right) = (0.5, 0.5)$, and 96.67% at $\left(\gamma, \frac{\rho_{\mathrm{E}}}{\rho_u}\right) = (0.5, 1)$. The similar observation, however, does not hold for the fourth SVM classifier (based on the sigmoid kernel) in Table VII, because we have 3.33% at $\left(\frac{\rho_{\mathrm{E}}}{\rho_u}, \gamma\right) = (1, 5)$ and 30% at $\left(\frac{\rho_{\mathrm{E}}}{\rho_u}, \gamma\right) = (0.1, 5)$. Looking into the accuracy in the sigmoid kernel case, we can find that it has less stability than the remaining kernels. In fact, the sigmoid kernel seems very sensitive to the change of γ.

Also in Table VII, the most stable and accurate scenarios are corresponding to the linear and RBF kernels, in which the linear kernel is independent of γ. As such, when considering the impact of γ on the accuracy, we suggest examining the RBF kernel other than the polynomial and sigmoid kernels. For the RBF kernel, if γ takes a small value, then training samples are considered similar; in contrast, if γ takes a large value, then there is less similarity among training samples. Through numerical results in Table VII, one can confirm again this observation. For example, at a fixed value of $\frac{\rho_{\mathrm{E}}}{\rho_u}$, the accuracy increases when γ decreases. In addition, the accuracy increases with $\frac{\rho_{\mathrm{E}}}{\rho_u}$. These observations allow us to reach the valuable insight in Remark 5.

Remark 5. *For SVM models, if Eve uses low transmit power to send $\mathbf{p}_E$ to the AP (i.e., if ρ_E decreases), then the SVM parameter γ should be small. We can understand that if Eve transmits $\mathbf{p}_E = \mathbf{p}_k$ with low power, she may try to make her signals similar to the signals from user k such that the AP fails to detect her presence. As mentioned above, to cope with the similarity among samples (which are created by handling the received signals at the AP), we set γ to a small value.*

In Table VIII, we record that except for the linear kernel, which is independent of γ, the most stable classifiers are related to the polynomial kernel. At $\frac{\rho_{\mathrm{E}}}{\rho_u} = 0.1$, the RBF seems to be better than the polynomial and sigmoid kernels. However, at $\frac{\rho_{\mathrm{E}}}{\rho_u} = 1$, the 3 considered kernel functions do not show huge difference in performance. Note that the decrease in γ will lead to lower detection rate. This observation contrasts with the observation for the SVM case.

E. Over-fitting problems: The impact of γ

In Figure 10, we make a comparison among four different sub-cases corresponding to $\gamma = \{0.05, 1, 20, 400\}$. The total number of training samples is equal to $T_{tot} = 2\widehat{T} = 400$. System parameters are the same as those in Table VI. Figure 10 illustrates the transformation of models when γ increases. With $\gamma = 400$, we face an over-fitting problem due to the fact that the fourth model learns so well and becomes too detailed.

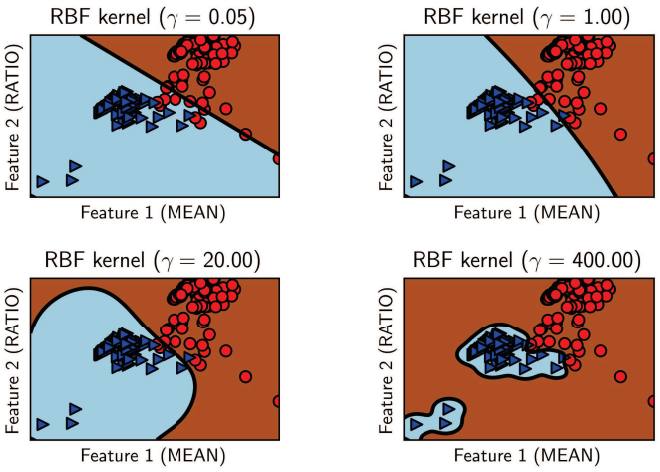

Fig. 10. 4 trained SVM models correspond to 4 different values of γ in the case of RBF kernel (with $C = 1$). The cyan area and $\triangleright$ markers relate to (#0), while the brown area and $\circ$ markers relate to (#1).

VI. Conclusions

We have considered a wireless communication system that requires the uplink phase for authentication. Eve has been assumed to impersonate a legal user. To identify the presence of Eve, we have introduced the ATD and employed SVM/OC-SVM. The results have shown the following insights:

- i) The importance of formulating/defining features and converting received signals into those features. In particular, we have defined and compared three features, namely MEAN, RATIO and SUM.
- ii) The impact of selecting kernel functions and SVM/OC-SVM parameters. Throughout the paper, the sigmoid kernel seems to be the worst kernel, while the RBF kernel appears to be the best one in terms of accuracy and stability.
- iii) The impact of the length of both training and testing datasets on the accuracy. We have shown that when $\widehat{T}$ and T increase, the accuracy of the linear-kernel-based, RBF-kernel-based, and polynomial-kernel-based SVM (and OC-SVM) classifiers can be improved.
- iv) The impact of selecting γ in relation to the Eve's power has been presented (see Remark 5). We have also shown the impact of selecting γ in relation to over-fitting problems.

The data obtained through our framework can also be fed into other machine learning algorithms, such as Gaussian mixture, random forest and isolation forest. So far, it has remained an open issue when considering those algorithms for the PLS and making a holistic comparison among them.

References

[1] Y. Shiu, S. Y. Chang, H. Wu, S. C.-H. Huang, and H. Chen, "Physical layer security in wireless networks: A tutorial," *IEEE Wireless Commun.*, vol. 18, no. 2, pp. 66–74, Apr. 2011.

[2] D. Kapetanovic, G. Zheng, and F. Rusek, "Physical layer security for massive mimo: An overview on passive eavesdropping and active attacks," *IEEE Commun. Mag.*, vol. 53, no. 6, pp. 21–27, June 2015.

[3] A. Al-nahari, "Physical layer security using massive multiple-input and multiple-output: passive and active eavesdroppers," *IET Communications*, vol. 10, no. 1, pp. 50–56, 2016.

[4] Y. Wu, R. Schober, D. W. K. Ng, C. Xiao, and G. Caire, "Secure massive MIMO transmission with an active eavesdropper," *IEEE Transactions on Information Theory*, vol. 62, no. 7, pp. 3880–3900, July 2016.

[5] T. M. Hoang, H. Q. Ngo, T. Q. Duong, H. D. Tuan, and A. Marshall, "Cell-free massive MIMO networks: Optimal power control against active eavesdropping," *IEEE Trans. on Commun.*, 2018, to appear.

[6] Y. Zou, J. Zhu, X. Wang, and L. Hanzo, "A survey on wireless security: Technical challenges, recent advances, and future trends," *Proceedings of the IEEE*, vol. 104, no. 9, pp. 1727–1765, Sep. 2016.

[7] W. Hou, X. Wang, J. Chouinard, and A. Refaey, "Physical layer authentication for mobile systems with time-varying carrier frequency offsets," *IEEE Trans. on Commun.*, vol. 62, no. 5, pp. 1658–1667, May 2014.

[8] L. Xiao, L. J. Greenstein, N. B. Mandayam, and W. Trappe, "Using the physical layer for wireless authentication in time-variant channels," *IEEE Trans. on Wireless Commun.*, vol. 7, no. 7, pp. 2571–2579, July 2008.

[9] L. Xiao, Y. Li, G. Han, G. Liu, and W. Zhuang, "PHY-layer spoofing detection with reinforcement learning in wireless networks," *IEEE Transactions on Vehicular Technology*, vol. 65, no. 12, pp. 10 037–10 047, Dec. 2016.

[10] X. Lu, X. Wan, L. Xiao, Y. Tang, and W. Zhuang, "Learning-based rogue edge detection in VANETs with ambient radio signals," in *IEEE Int. Conf. on Commun. (ICC)*, May 2018, pp. 1–6.

[11] N. Wang, T. Jiang, S. Lv, and L. Xiao, "Physical-layer authentication based on extreme learning machine," *IEEE Commun. Letters*, vol. 21, no. 7, pp. 1557–1560, July 2017.

[12] C. Pei, N. Zhang, X. S. Shen, and J. W. Mark, "Channel-based physical layer authentication," in *IEEE Global Commun. Conf.*, Dec. 2014, pp. 4114–4119.

[13] M. Esmalifalak, L. Liu, N. Nguyen, R. Zheng, and Z. Han, "Detecting stealthy false data injection using machine learning in smart grid," *IEEE Systems Journal*, vol. 11, no. 3, pp. 1644–1652, Sep. 2017.

[14] B. Chatterjee, D. Das, S. Maity, and S. Sen, "RF-PUF: Enhancing IoT security through authentication of wireless nodes using in-situ machine learning," *IEEE Internet of Things Journal*, 2018, to appear.

[15] A. Weinand, M. Karrenbauer, R. Sattiraju, and H. Schotten, "Application of machine learning for channel based message authentication in mission critical machine type communication," in *the 23rd European Wireless 2017*, Dresden, Germany, May 2017, pp. 342–346.

[16] I. Guyon, S. R. Gunn, M. Nikravesh, and L. Zadeh, *Feature Extraction, Foundations and Applications*. New York: Springer-Verlag, 2006.

[17] V. N. Vapnik, *The Nature of Statistical Learning Theory*. USA: Springer-Verlag, 1995.

[18] N. I. Sapankevych and R. Sankar, "Time series prediction using support vector machines: A survey," *IEEE Compu. Intell. Magazine*, vol. 4, no. 2, pp. 24–38, May 2009.

[19] C. J. C. Burges, "A tutorial on support vector machines for pattern recognition," *Knowledge Discovery and Data Mining*, vol. 2, no. 2, pp. 121–167, 1998.

[20] S. Abe, *Support Vector Machines for Pattern Classification*. USA: Springer-Verlag, 2005.

[21] F. Perez-Cruz and O. Bousquet, "Kernel methods and their potential use in signal processing," *IEEE Signal Process. Magazine*, vol. 21, no. 3, pp. 57–65, May 2004.

[22] B. Scholkopf and A. J. Smola, *Learning with Kernels: Support Vector Machines, Regularization, Optimization, and Beyond*. USA: The MIT Press, 2002.

[23] C. Cortes and V. Vapnik, "Support-vector networks," *Machine Learning, Springer*, vol. 3, no. 20, pp. 273–29, Sep. 1995.

[24] C. M. Bishop, *Pattern Recognition and Machine Learning*. New York: Springer-Verlag, 2006.

[25] L. M. Manevitz and M. Yousef, "One-class SVMs for document classification," *Journal of Machine Learning Research*, vol. 2, pp. 139–154, Dec. 2001.

[26] Y. Wang, J. Wong, and A. Miner, "Anomaly intrusion detection using one class SVM," in *The Fifth Annual IEEE SMC Info. Assurance Workshop*, West Point, NY, June 2004, pp. 358–364.

[27] B. Scholkopf, J. C. Platt, J. Shawe-Taylor, A. J. Smola, and R. C. Williamson, "Estimating the support of a high-dimensional distribution," *Neural Computation*, vol. 13, no. 7, pp. 1443–1471, July 2001.

[28] Y. Wu, R. Schober, D. W. K. Ng, C. Xiao, and G. Caire, "Secure massive MIMO transmission in presence of an active eavesdropper," in *IEEE Int. Conf. Commun. (ICC)*, London, UK, Jun. 2015, pp. 1434–1440.

[29] O. Chapelle, "Training a support vector machine in the primal," *Neural Comput.*, vol. 19, no. 5, pp. 1155–1178, 2007.

[30] C.-C. Chang and C.-J. Lin, "LIBSVM: A library for support vector machines," *ACM Trans. Intell. Syst. Technol.*, vol. 2, no. 3, 2011. [Online]. Available: https://www.csie.ntu.edu.tw/~cjlin/papers/libsvm

[31] A. Abdiansah and R. Wardoyo, "Time complexity analysis of support vector machines (SVM) in LibSVM," *Int. J. Comput. Appl.*, vol. 128, no. 3, pp. 0975—8887, 2015.

[32] L. C. U. G. L. Grinblat and P. M. Granitto, "Abrupt change detection with one-class time-adaptive support vector machines," *Expert Syst. Appl.*, vol. 40, no. 18, pp. 7242–7249, 2013.

[33] J. Davis and M. Goadrich, "The relationship between precision-recall and ROC curves," in *Proc. of the 23rd Int. Conf. on Machine Learning*, ser. ICML '06. New York, NY, USA: ACM, 2006, pp. 233–240.

[34] T. Fawcett, "An introduction to ROC analysis," *Pattern Recognition Letters*, vol. 27, no. 8, pp. 861–874, July 2006, rOC Analysis in Pattern Recognition. [Online]. Available: http://www.sciencedirect.com/science/article/pii/S016786550500303X

[35] Y. Tang, Y. Zhang, N. V. Chawla, and S. Krasser, "SVMs modeling for highly imbalanced classification," *IEEE Trans. on Sys., Man, and Cyber., Part B (Cyber.)*, vol. 39, no. 1, pp. 281–288, Feb. 2009.